

Capacitive Transduction for Liquid Crystal-Based Sensors, Part I: Ordered System

Alaeddin Abu-Abed, *Student Member, IEEE*, Robert G. Lindquist, and Woo-Hyuck Choi

Abstract—In this paper, the theory for tracking the average molecular orientation of a liquid crystal (LC) material via capacitive sensing of anisotropic media is presented. The candidate LC sensor structure utilizes interdigital electrodes. Two capacitive measurements in orthogonal direction can track the director axis of nematic LC material in a homogenous ordered LC film. The sensitivity for the sensor at different alignments is studied. The candidate sensors have been fabricated and experimentally verified. Both experimental and calculated values for capacitances of selected interdigital fingers sensor structures are presented.

Index Terms—Biosensors, capacitive sensing, chemical sensors, liquid crystal (LC).

I. INTRODUCTION

RECENTLY, nematic liquid crystal (LC) systems have proven to be excellent candidates for reliable, sensitive, low cost sensors for chemical and biological agents [1]–[10]. In LC-based sensors, the presence of a chemical or biological agent causes a change in the alignment of the LC material [11]–[19]. Due to the collective behavior and the highly anisotropic properties of LC molecules, detection of very low levels of chemical and biological agents are possible [11]–[19]. Researchers from the University of Wisconsin have demonstrated surface-driven orientational changes of LC molecules in both chemical and biological systems with sensitivity levels as low as ten parts per billion. In addition, nematic LCs have also been used to amplify protein binding events [11], [12]. In each of these examples, visual inspection or optical microscopy has been used to sense the deformations within the LC material. In this paper, an alternative transduction mechanism is presented based on capacitive measurements in highly anisotropic media. The innovation of this work is the first ever demonstrated capacitive transduction in an LC sensor.

Switching to a capacitive transduction mechanism from the present optical techniques in LC-based sensors offers some noteworthy advantages. First, it provides greater insight into the fundamental distortion occurring in the LC film due to the presence of chemical and biological agents. Rather than simply sensing the LC distortion, capacitive techniques offer the ability to identify and track the average deformation [20].

Manuscript received June 21, 2007; revised August 13, 2007; accepted August 14, 2007. This work was supported in part by the National Science Foundation (NSF) under Award BES-0428073.

The authors are with the Department of Electrical and Computer Engineering, University of Alabama at Huntsville, Huntsville, AL 35899 USA (e-mail: abuabea1@eng.uah.edu; lindquis@ece.uah.edu).

Color versions of one or more of the figures in this paper are available online at <http://ieeexplore.ieee.org>.

Digital Object Identifier 10.1109/JSEN.2007.908504

Second, capacitive sensing does not require visual inspection and consumes little power which makes it ideal for a remotely deployable sensor. Third, the removal of the optical transparency requirement of the substrate allows for a broader class of substrate selection. For instance, one of the substrates could be silicon to allow for integration of electronics and the other could be a porous ceramic to help facilitate the movement of chemical or biological agents to the sensing interface. These advantages and others provide a compelling argument to investigate the capacitive sensing approach.

In this paper, the theory for tracking the average molecular orientation of an LC material via capacitive sensing of anisotropic media is presented. Moreover, the LC material will assume to be homogeneous and, thus, can be treated as an ordered uniaxial crystal. In some cases, the LC film will be partially disordered. This is especially true when the temperature is elevated close to the LC phase transition temperature. An upcoming paper presently in preparation will address the issue of a partially disorder LC film in which the LC can be treated as an inhomogeneous material.

Background information for LC sensors for tracking director axis orientation via capacitive sensing and for practical sensor designs is provided in Section II. The theory to model capacitive changes in homogeneous anisotropic media using 2-D finite difference method is given in Section III. Section IV contains simulation and experimental results and discussion of these results, while the conclusion is presented in Section V.

II. BASIC CONCEPTS

In nematic LC-based sensors, the molecular alignment in LC film is altered in response to some environmental condition. For most chemical and biological sensors, the orientational behavior of LCs near surfaces is exploited. A homeotropic alignment will change to homogeneous as was demonstrated by Abbott and Shah [11] in detecting parts-per-billion concentration of dimethylmethylphosphonate (DMMP). Another example is when a homogeneous alignment at a given angle will rotate to a homogeneous alignment at a different angle as shown in [11]. Due to the collective behavior of molecules forming LCs, a change in the structure at the surface caused by the binding of a chemical or biological agent is amplified into a significant change in the average molecular alignment of the LC film. The mechanisms for sensing biological and chemical agents and its impact on the alignment of the film is well described in the literature and the readers are referred to the cited references for details.

The capacitive transduction in LC-based sensors exhibits a change in capacitance in response to a change in the molecular

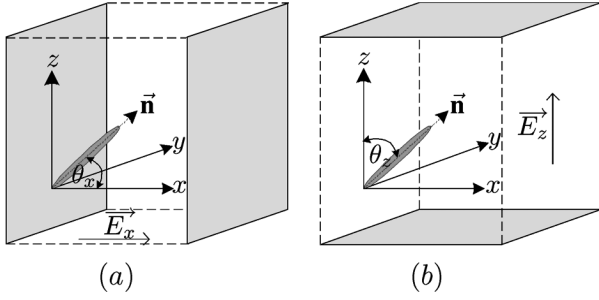


Fig. 1. The cube model illustrating the director axis tracking.

deformation in the LC film. The objective of this paper is to provide insight into the molecular behavior inside the LC film and to illustrate how capacitive measurements can uniquely track the average molecular distortion, or the director axis, in an ordered LC film. As previously mentioned, the LC film will be represented locally as an ordered uniaxial crystal that exhibits two electrical permittivities, the parallel permittivity, ϵ_{\parallel} , for the electric field traveling in parallel with the director axis, and the perpendicular permittivity ϵ_{\perp} for the electric field traveling in perpendicular with the director axis. The permittivity tensor, ϵ_n , in the director axis principal coordinate system is given by [22]

$$\epsilon_n = \begin{bmatrix} \epsilon_{\perp} & 0 & 0 \\ 0 & \epsilon_{\perp} & 0 \\ 0 & 0 & \epsilon_{\parallel} \end{bmatrix}. \quad (1)$$

The following sections describe how capacitive measurements can uniquely define the axis of symmetry of a uniaxial crystal under ideal and practical electrode configurations.

A. Capacitive Sensing

A simplified view for sensing the axis of symmetry for a uniaxial crystal using capacitive measurements can be illustrated by demonstrating a cube filled with a rod-like nematic LC material and considering two parallel plate capacitance measurements, as shown in Fig. 1. First, the electrodes are positioned to provide a transverse capacitance in the x -direction, as in Fig. 1(a), and then moved to provide a transverse capacitance in the z -direction, as in Fig. 1(b). The director axis is denoted by \vec{n} , where without loss of generality, the director axis has unit length $|\vec{n}| = 1$. The capacitance between the parallel plates is given by

$$C_i = \frac{\epsilon_{\text{eff},i} \epsilon_0 A}{d} \quad (2)$$

in which $i = x, y, \text{ or } z$, $\epsilon_{\text{eff},i}$ is the effective relative permittivity of the LC material in the direction of the electric field, where the electric field is assumed to be in the i direction, ϵ_0 is the permittivity of the free space, A is the area of each plate, and d is the separation between the parallel plates. Let θ_x , θ_y , and θ_z be the angles between the director axis and the laboratory frame axes x , y , and z , respectively. When the electric field penetrates the LC film along with the i axis, it exhibits an effective permittivity given by

$$\epsilon_{\text{eff},i} = \epsilon_{\perp} \sin^2 \theta_i + \epsilon_{\parallel} \cos^2 \theta_i \quad (3)$$

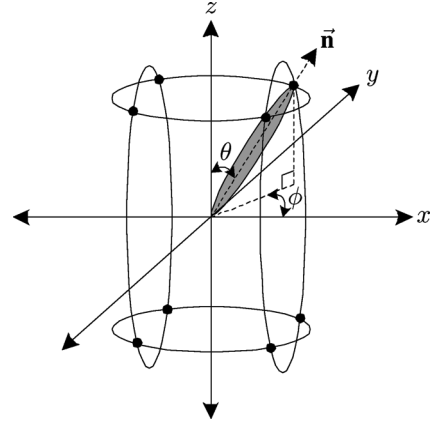


Fig. 2. A unique solution is shown in each octant.

where θ_i could be either θ_x , θ_y , or θ_z . These angles can be defined according to the standard Euler's angles as follows, let the zenithal angle, θ , be the angle between the director axis and the z axis, where the azimuthal angle, ϕ , is the angle between the x axis and the projection of the director axis onto the $x-y$ plane. Therefore, $\theta_x = \cos^{-1}(\cos \phi \sin \theta)$, $\theta_y = \cos^{-1}(\sin \phi \sin \theta)$ and $\theta_z = \theta$. The director axis vector can be expressed in terms of θ and ϕ as

$$\vec{n} = \sin \theta \cos \phi \hat{x} + \sin \theta \sin \phi \hat{y} + \cos \theta \hat{z} \quad (4)$$

where the effective permittivities can be expressed in terms of θ and ϕ as

$$\begin{aligned} \epsilon_{\text{eff},x} &= \epsilon_{\perp} + \Delta\epsilon \sin^2 \theta \cos^2 \phi \\ \epsilon_{\text{eff},y} &= \epsilon_{\perp} + \Delta\epsilon \sin^2 \theta \sin^2 \phi \\ \epsilon_{\text{eff},z} &= \epsilon_{\perp} + \Delta\epsilon \cos^2 \theta \end{aligned} \quad (5)$$

where $\Delta\epsilon = \epsilon_{\parallel} - \epsilon_{\perp}$ is the dielectric anisotropy.

Since the effective permittivity depends on θ and ϕ , these angles can be determined by performing capacitance measurements. This test shows that only two capacitance measurements between two perpendicular electrodes are required to track the average orientation of the director axis of the ordered nematic LC material.

Although two capacitance measurements are required to define the director axis vector, these measurements will lead to eight different solutions of θ and ϕ . For example, take the measured capacitances in the x and z directions; all the solutions that satisfy each of these measurements are shown in Fig. 2. Since \vec{n} and $-\vec{n}$ are indistinguishable, the upper and lower circles in Fig. 2 represent all the solutions that have the same θ_z , where the right and left circles represent all the solutions that have the same θ_x . The intersections of these circles lead to eight different solutions (these solutions can also be obtained for this particular case by solving $\epsilon_{\text{eff},x}$ and $\epsilon_{\text{eff},z}$ for θ and ϕ). These solutions are (θ, ϕ) , $(\theta, -\phi)$, $(\theta, \pi + \phi)$, $(\theta, \pi - \phi)$, $(\pi - \theta, \phi)$, $(\pi - \theta, -\phi)$, $(\pi - \theta, \pi + \phi)$ and $(\pi - \theta, \pi - \phi)$, where θ and ϕ are in the range $\in [0, \pi/2]$. It is noticed that each pair belongs to a different octant, which means the solution is unique in any octant.

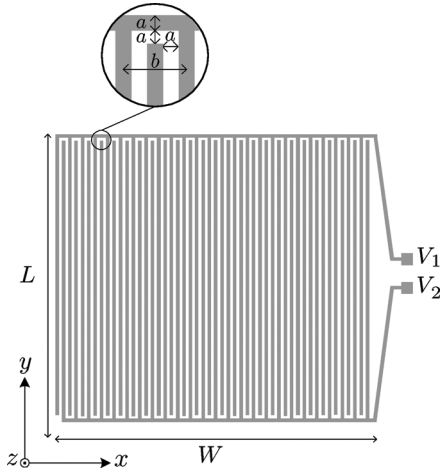


Fig. 3. Top view of a $W \times L$ interdigitated electrodes sensor.

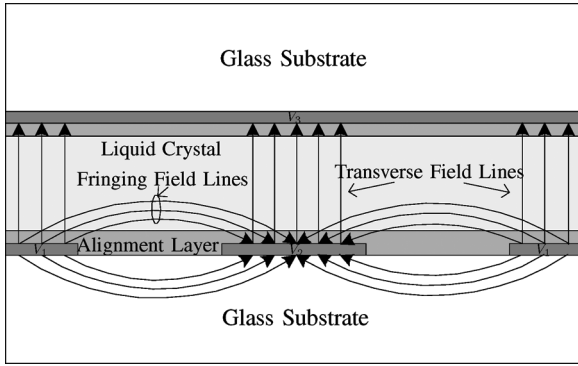


Fig. 4. A cross section of one unit cell of Structure I in the $x-z$ plane.

B. Practical Implementation

Although the cube discussed above is appropriate to illustrate the concept of sensing the director axis using capacitance measurements, the cube is not practical for LC materials since LCs are typically in the form of films. A possible electrode design for tracking the director axis is shown in Figs. 3 and 4. This design will be called Structure I. In Fig. 3, a top view of the sensor in the $x-y$ plane is shown, while Fig. 4 shows a cross section of one unit cell of the sensor in the $x-z$ plane. A continuous electrode is deposited on a glass substrate and interdigitated electrodes on another glass substrate. The LC film of thickness d is sandwiched between the two substrates. In fact, Fig. 4 shows one unit cell pattern, when this pattern is repeated, the resulting structure is called the “interdigital” structure, as in Fig. 3.

By applying various electrical potentials to the three electrodes, both fringing and transverse capacitances can be measured as those shown in Fig. 5. In Fig. 5, the transverse capacitances are denoted by $C_T/2$, where the fringing capacitance is denoted by C_F . When V_1 and V_2 are tied together, the transverse capacitance can be measured between the electrode V_1 (or V_2) and V_3 . Measuring the fringing capacitance requires fringing electric field between V_1 and V_2 , this can be achieved when $V_1 \neq V_2$. It is important to notice that the potentials used to measure the capacitance in this sensor should not exceed the Freedericksz transition electric field strength (~ 400 volts/cm) or the LC molecules will rotate as a function of the potential [24].

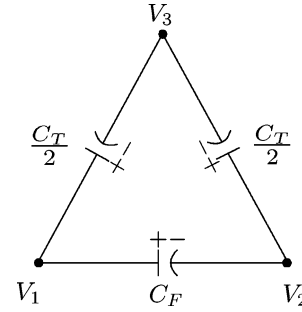


Fig. 5. The symbolic representation of the transverse and fringing capacitance between the electrodes of the Structure I.

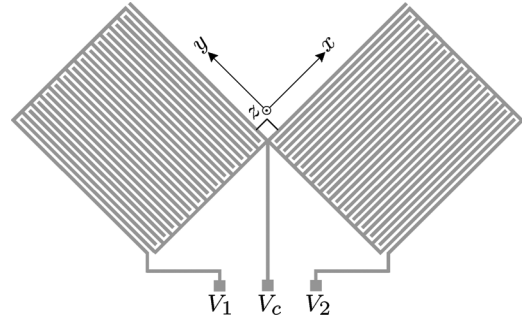


Fig. 6. Top view of Structure II.

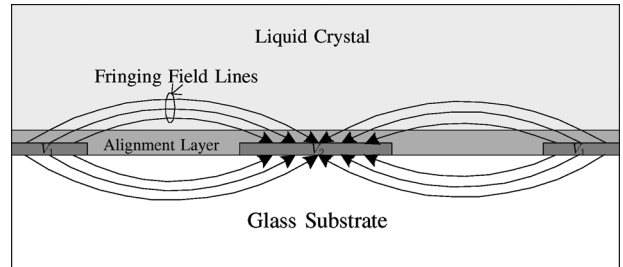


Fig. 7. A cross section of one unit cell of Structure II in the $x-z$ plane.

The results will show later that the transverse capacitance depends only on θ , where the fringing capacitance depends on both θ and ϕ . By measuring the transverse capacitance, the angle θ could be determined while measuring the fringing one (where θ is available), the angle ϕ could be determined.

Another useful electrode design is Structure II which consists of two perpendicular interdigitated cells. A top view is shown in Fig. 6, while a cross section of one unit cell is shown in Fig. 7. In this structure, two perpendicular interdigitated cells allow tracking of the director axis, where the top electrode is not required. In the absence of a top interface, the LC molecules will only maintain a controlled alignment near the surface. Using the spacing between the interdigitated electrodes to limit the electric field penetration depth, only LC layer(s) close to the electrodes can be monitored. For example, as reported by Kim and Lee [21], 95% of the electric field lines will penetrate only $\sim 11 \mu\text{m}$ of the LC film when $a = 4 \mu\text{m}$. Using this structure allows measuring two independent fringing capacitances, each capacitance depends on both θ and ϕ . These capacitances will be called $C_{F1}(\theta, \phi)$ and $C_{F2}(\theta, \phi)$, as illustrated in Fig. 8.

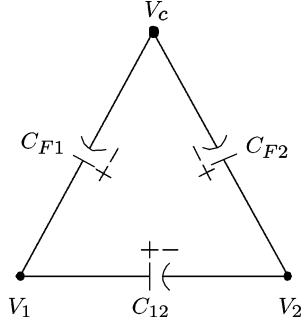


Fig. 8. The symbolic representation of the fringing capacitance between the electrodes of Structure II.

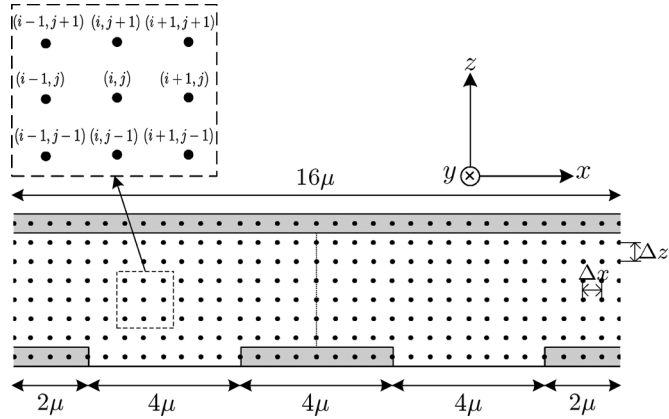


Fig. 9. Graphical display of one unit cell in a potential field that is divided into $\Delta x \times \Delta z$ regions to solve Maxwell's equation for $V_{i,j}$.

III. THEORY

Although some analytical techniques, such as conformal mapping, are used to derive a closed form for the interdigitated structure capacitance associated with homogenous and isotropic material such as conformal mapping, there is no such formula to calculate this capacitance in the presence of anisotropic material. In this section, a numerical method will be used to calculate the transverse and fringing capacitances in the presence of an LC material. Since the LC film is assumed to be anisotropic, the electric field in LC film satisfies Maxwell's equation [12]

$$\nabla \cdot (\epsilon \vec{E}) = 0 \quad (6)$$

where ϵ is the permittivity tensor and \vec{E} is the electric field, both in the laboratory frame coordinate system. Maxwell's equation will be solved in two regions, the uniaxial LC film and the glass substrate. Fig. 9 shows a one unit cell mesh grid used to solve this problem.

The reason for choosing the unit cell, as shown in Fig. 9, rather than half of it is that the electric field lines the right-half side of this unit cell is not always symmetrical to electric field lines the left half side when uniaxial LC film is used. For example, Fig. 10 shows the electric field vector and the equipotential lines for both structures when $\theta = \phi = 45^\circ$. The electric field \vec{E} is represented in arrows where the directions of the arrows represent the direction of the electric field at the points and the magnitudes of the arrows represent the magnitude of

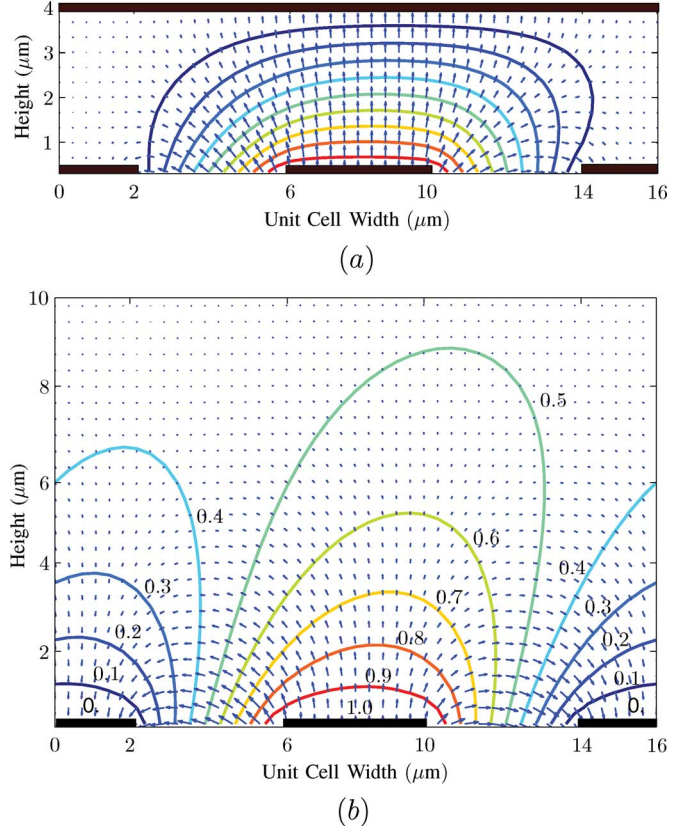


Fig. 10. Asymmetry in the electric field vectors and equipotential lines when $\theta = \phi = 45^\circ$ in one unit cell of the sensor structure (a) with top electrode (Structure I) and (b) without top electrode (Structure II).

the electric field at these points. The solid curves represent the equipotential lines. It is obviously shown that the electric field as well as the equipotential lines in the right-half side of Fig. 10 are not symmetrical to those in the left-half side.

The analysis is applied to one unit cell, and by making full use of symmetry, the capacitance for the whole structure can be evaluated. Let the capacitance per unit cell per length is C_{uc} and the capacitance of the edge is neglected, then the total capacitance of the interdigital sensor is given by

$$C_{\text{TOTAL}} = C_{uc}(N - 1)L \quad (7)$$

where N is the number of unit cells and L is the length of the electrode fingers.

A. Solving Equation (6) Inside the LC Film

Since the LC film is anisotropic material, the permittivity ϵ is a tensor represented by a 3×3 matrix. Due to the uniaxial nature of the LC film, the permittivity tensor is symmetrical. Simplifying (6) will end up with a simple partial differential equation

$$\epsilon_{xx} \frac{\partial^2 V(x, z)}{\partial x^2} + 2\epsilon_{xz} \frac{\partial^2 V(x, z)}{\partial x \partial z} + \epsilon_{zz} \frac{\partial^2 V(x, z)}{\partial z^2} = 0 \quad (8)$$

where

$$\begin{aligned} \epsilon_{xx} &= \epsilon_{\perp} + \Delta\epsilon \sin^2 \theta \cos^2 \phi \\ 2\epsilon_{xz} &= \Delta\epsilon \sin 2\theta \cos \phi \\ \epsilon_{zz} &= \epsilon_{\perp} + \Delta\epsilon \cos^2 \theta. \end{aligned} \quad (9)$$

The partial differential equation in (8) will be solved for the potential $V(x, z)$ at random point, (i, j) , using the finite difference method (FDM). By applying FDM to (8), the potential at the (i, j) node is given by

$$V_{i,j} = A_x(V_{i+1,j} + V_{i-1,j}) + A_z(V_{i,j+1} + V_{i,j-1}) + A_{xz}(V_{i+1,j+1} - V_{i+1,j-1} - V_{i-1,j+1} + V_{i-1,j-1}) \quad (10)$$

where

$$\begin{aligned} A_x &= 0.5\epsilon_{xx}(\Delta z)^2 / (\epsilon_{xx}(\Delta z)^2 + \epsilon_{zz}(\Delta x)^2) \\ A_z &= 0.5\epsilon_{zz}(\Delta x)^2 / (\epsilon_{xx}(\Delta z)^2 + \epsilon_{zz}(\Delta x)^2) \\ A_{xz} &= 0.25\epsilon_{xz}\Delta x\Delta z / (\epsilon_{xx}(\Delta z)^2 + \epsilon_{zz}(\Delta x)^2). \end{aligned} \quad (11)$$

B. Solving Equation (6) Inside the Glass Substrate

The glass is an isotropic material with dielectric constant ϵ_r . Therefore, Maxwell's equation in (8) is simplified to

$$\frac{\partial^2 V(x, z)}{\partial x^2} + \frac{\partial^2 V(x, z)}{\partial z^2} = 0. \quad (12)$$

Solving (12) for $V(x, z)$ at the (i, j) node gives

$$V_{i,j} = \frac{0.5(\Delta x)^2(\Delta z)^2}{(\Delta x)^2 + (\Delta z)^2} \left[\frac{V_{i+1,j} + V_{i-1,j}}{(\Delta x)^2} + \frac{V_{i,j+1} + V_{i,j-1}}{(\Delta z)^2} \right]. \quad (13)$$

C. Calculating the Capacitance

The capacitance per unit cell per length between any two electrodes can be calculated as follows:

$$C_{uc} = \frac{Q}{V_d} \quad (14)$$

where V_d is the potential difference between the two electrodes and Q is the charge per unit length which could be calculated by applying Gauss's law to a closed path ℓ enclosing the electrode [23]

$$Q = \oint_{\ell} \epsilon \vec{E} \cdot d\vec{\ell}. \quad (15)$$

Since the parasitic capacitances in both structures are very small ($\sim 10^{-15}$ Farad) and neglected with respect to the fringing and transverse capacitances ($\sim 10^{-12}$ Farad), they are ignored in the capacitance modeling.

IV. SIMULATION AND EXPERIMENTAL RESULTS

In this section, simulation results are presented to provide insight into capacitive transduction for both structures. First, the capacitances in both structures as functions of the director axis orientation are given. Second, numerical examples are given to illustrate the link between the capacitance measurements and the director axis orientation. Third, the sensitivity of the capacitance as a function of the director axis orientation is specified to aid in optimizing the electrode structure and initial orientation. Finally, experimental results are presented and compared with the calculated ones.

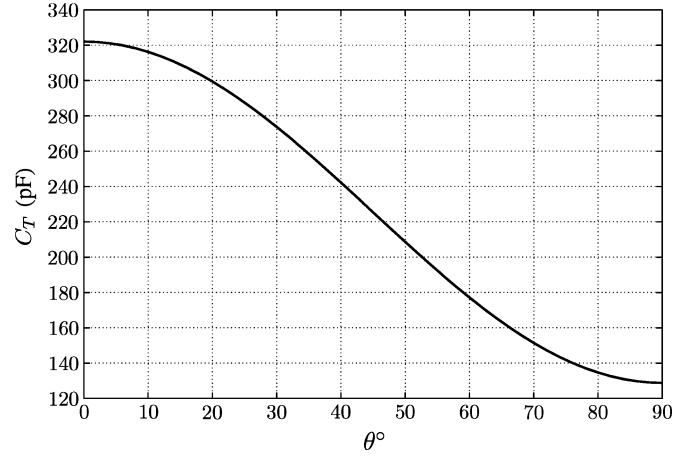


Fig. 11. Transverse capacitance of Structure I, C_T in pF, as a function of θ .

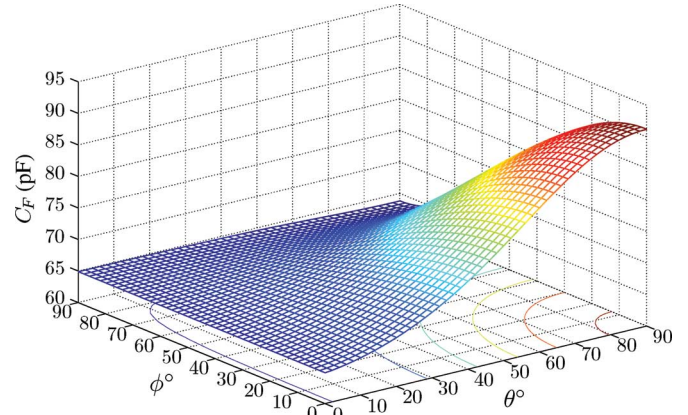


Fig. 12. Fringing capacitance of Structure I, C_F in pF, as a function of θ and ϕ .

For Structure I with $L = W = 4$ mm, $a = 4$ μ m and when a 4- μ m-thick 5CB LC film is used, the transverse capacitance as a function of θ is shown in Fig. 11 where the fringing capacitance as a function of θ and ϕ is shown in Fig. 12. As a numerical example to show how this structure could be used to track the director axis orientation, i.e., (θ, ϕ) , when the measured capacitances are $C_T = 251.5$ pF and $C_F = 66.5$ pF. From Fig. 11, it is shown that the θ angle corresponding to 251.5 pF is $\theta = 37.2^\circ$, while from Fig. 12, the ϕ angle corresponding to $\theta = 37.2^\circ$ and $C_F = 66.5$ pF is $\phi = 64.8^\circ$.

In the case of Structure II with $L = W = 4$ mm, $a = 4$ μ m and when 5CB LC film is used, the two fringing capacitances C_{F1} and C_{F2} , as functions of θ and ϕ are shown in Figs. 13 and 14, respectively. This structure also with two fringing capacitance measurements could be used to track the director axis. As an example, for the fringing capacitances $C_{F1} = 111.14$ pF and $C_{F2} = 93.82$ pF, the solutions that satisfy each one of these measurements are shown in Fig. 15. Although there are many different solutions which satisfies each one of these capacitances, there is only one solution that satisfies both. This solution is the intersection between both curves shown in Fig. 15 which is $(68.2^\circ, 24.7^\circ)$.

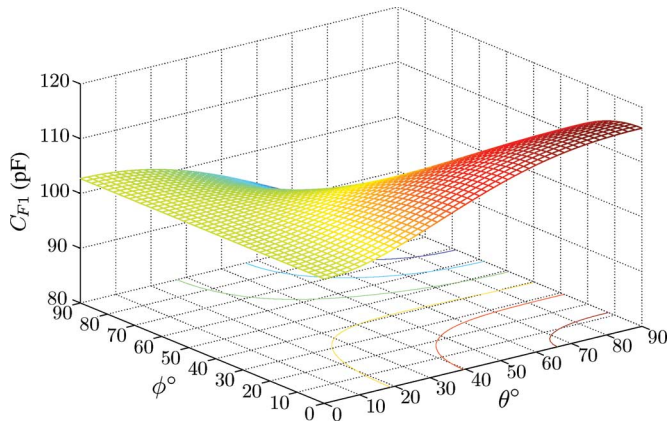


Fig. 13. Fringing capacitance of Structure II C_{F1} in pF as a function of θ and ϕ .

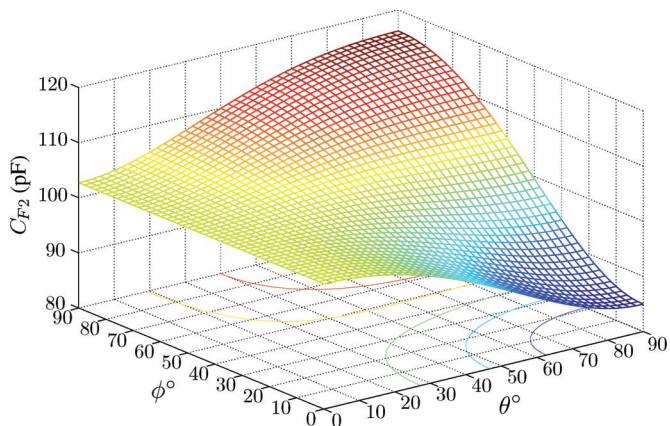


Fig. 14. Fringing capacitance of Structure II, C_{F2} in pF, as a function of θ and ϕ .

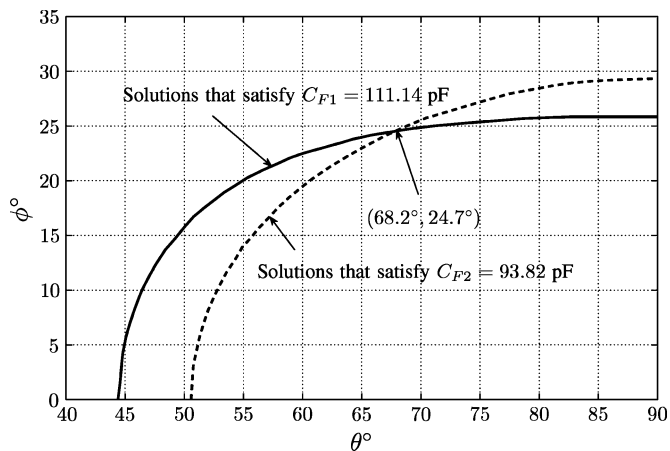


Fig. 15. Results of an example illustrates the tracking of director axis orientation using Structure II when $C_{F1} = 111.14$ pF and $C_{F2} = 93.82$ pF.

A prior knowledge of how the orientation of the LC molecules will likely reorient in response to some environmental stimulus is critical to optimizing the performance of the sensor. The electrode structure and the initial state of orientation impact the sensitivity. For instance, a change in the zenithal angle θ , which is anticipated with alignment changes between homeotropic and homogeneous, will result in a large change to the transverse capacitance in Structure I. However, a change in the azimuthal

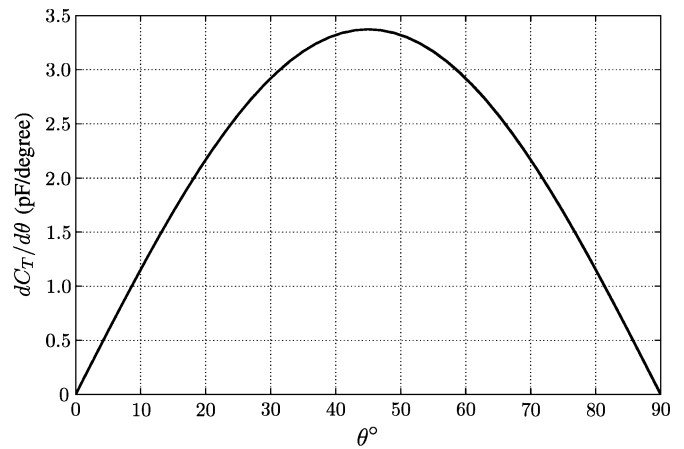


Fig. 16. Sensitivity, in pF/degree, of the transverse capacitance of Structure I.

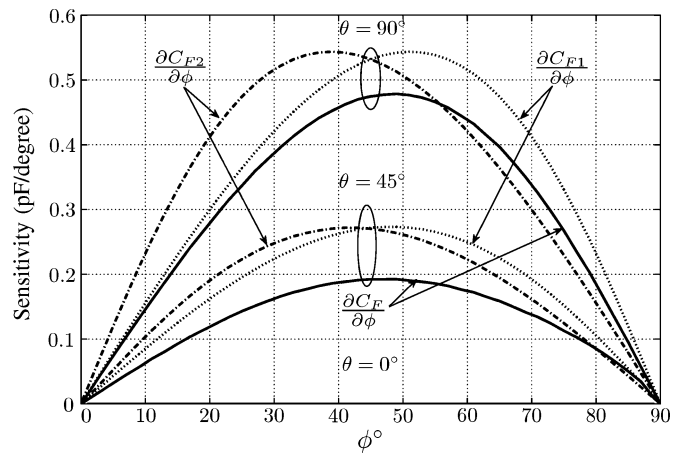


Fig. 17. Sensitivity, in pF/degree, of the fringing capacitance for different values of θ , as a function of ϕ , for both structures.

angle, ϕ , seen when the homogeneous alignment rotates provides no change in the transverse capacitance in that structure. The sensitivity of the transverse capacitance is shown in Fig. 16. The maximum occurs at $\theta = 45^\circ$ and is independent of ϕ . The sensitivity of the fringing field capacitance for both electrode structures is a function of both the zenithal and azimuthal angles. Fig. 17 illustrates the sensitivity of the fringing field capacitance as a function of ϕ given the θ is 0° , 45° , and 90° . As expected, the sensitivity is a maximum when $\theta = 90^\circ$ (homogeneous alignment) and is insensitive at $\theta = 0^\circ$ (homeotropic alignment). Fig. 18 illustrates the sensitivity of the fringing capacitance as a function of the θ given the $\phi = 0^\circ$. Although Structure II offers some advantages over Structure I because the assembly of the top electrode is not required, results show that Structure II has less sensitivity when the molecules change from homeotropic to homogenous alignment. In Fig. 19, we observe, the change in the fringing capacitance C_F when the molecules' initial orientation is a homogeneous alignment at $\phi_o = 35^\circ$ with respect to the x axis. When all the molecules experience 90° clockwise (CW) rotation to another homogeneous alignment (the upper curve), the capacitance passes through maximum. When the molecules experience 90° counter clockwise rotation

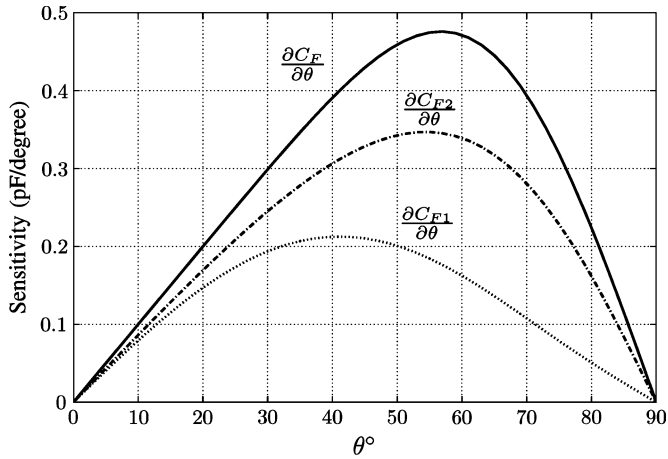


Fig. 18. Sensitivity, in pF/degree, of the fringing capacitance when the director axis changes from homeotropic to homogenous with $\phi = 0$, for both structures.

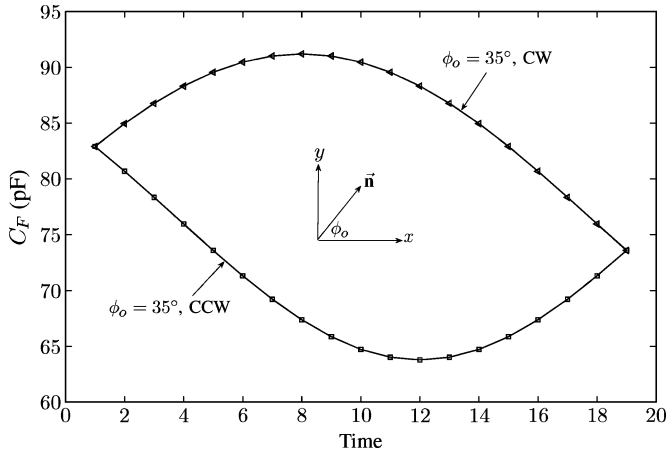


Fig. 19. Change in fringing capacitance C_F from an initial homogenous alignment at $\phi_o = 35^\circ$ by rotating 90° CW and CCW.

(CCW) to another homogenous alignment (the lower curve), the capacitance passes through minimum.

The behavior of the previously discussed sensor in the presence of nematic LC film was investigated experimentally. Interdigitated electrodes structures with $L = 5.5$ mm, $W = 5$ mm, and $a = 10 \mu\text{m}$ have been fabricated and tested. Different thicknesses of BL006 (Merck) LC films have been used. The molecules were aligned to behave in a homeotropic alignment, where $\theta = 0^\circ$ and in a homogenous alignment, where $\theta = 90^\circ$, where ϕ is set to different values between 0° and 90° . Test cells of this fabricated LC-based sensor are shown in Fig. 20. The capacitances at these angles were calculated numerically and measured experimentally by an Agilent 4263B LCR meter. For Structure I, the measured versus the calculated fringing capacitance as a function of ϕ with a $13 \mu\text{m}$ homogeneously aligned BL006 film is shown in Fig. 21. For Structure II, a thick enough LC film is used. When the molecules are in homeotropic alignment, the fringing capacitance is independent of ϕ . In this case, the average measured capacitance is 74.2 pF compared with the calculated one 70.7 pF. For the homogenous alignment cases, both the calculated and measured capacitances are shown in Fig. 22.

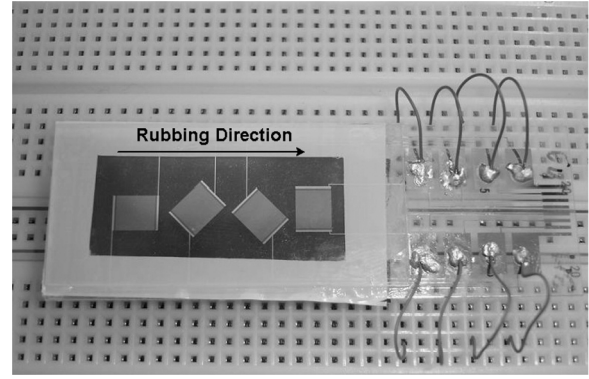


Fig. 20. Test cells of the LC-based sensor.

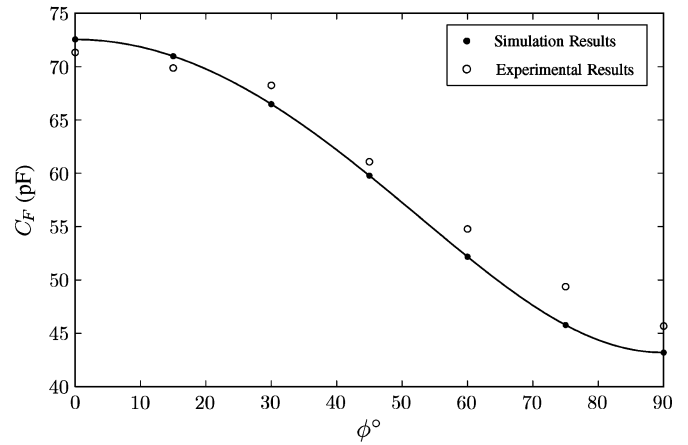


Fig. 21. Experimental and calculated results of Structure I for a homogeneous alignment when $\theta = 90^\circ$.

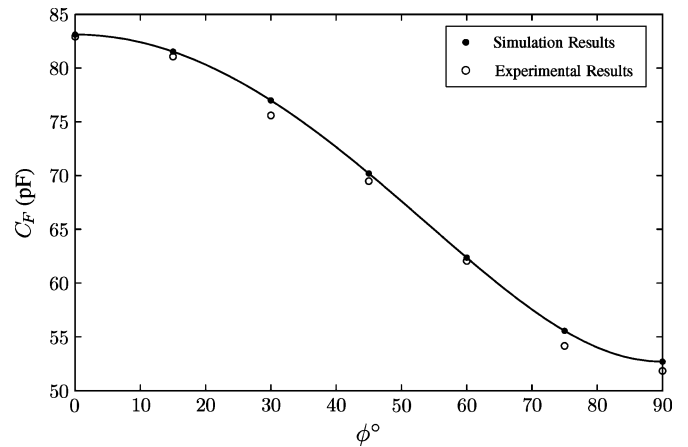


Fig. 22. Experimental and calculated results of Structure II for a homogeneous alignment when $\theta = 90^\circ$.

V. CONCLUSION

The method of capacitive transduction for LC-based sensors has been presented and tested. Sensors with interdigitated electrodes can be used to track the director axis of an ordered nematic LC film. Two capacitance measurements are needed to track the average alignment of the LC molecules. However, the electrode structures which were given in this paper are not the only possibility and may not be the ideal structure for every

sensor. The follow-up paper will focus on partially disordered LC films, where the molecules may have different orientations inside the LC film. In this case, capacitive transduction will be used to track the average molecular orientation (the director axis) as well as the degree of disorder inside the LC film.

REFERENCES

- [1] D. Villalta, P. B. Romelli, C. Savina, N. Bizzaro, R. Tozzoli, E. Tonutti, A. Ghirardello, and A. Doria, "Anti-dsDNA antibody avidity determination by a simple reliable ELISA method for SLE diagnosis and monitoring," *Lupus*, vol. 12, no. 1, pp. 31–36, 2003.
- [2] J. Chung, S. Park, D. Kim, J. Rhim, I. Kim, I. Choi, K. Yi, S. Ryu, P. Suh, D. Chung, Y. Bae, Y. Shin, and S. Park, "Identification of antigenic peptide recognized by the anti-JL1 leukemia-specific monoclonal antibody from combinatorial peptide phage display libraries," *J. Cancer Research and Clinical Oncology*, vol. 128, no. 12, pp. 641–649, 2002.
- [3] S. Poole, Y. Mistry, C. Ball, D. Gaines, E. Rose, L. P. Opie, G. Tucker, and M. Patel, "A rapid 'one-plate' in vitro test for pyrogens," *Journal of Immunological Methods*, vol. 274, no. 1–2, pp. 209–220, 2003.
- [4] M. C. Kibbey, D. MacAllan, and J. W. Karaszkiwicz, "Novel electrochemiluminescent assays for drug discovery," *J. Assoc. Lab. Autom.*, vol. 5, no. 1, pp. 45–48, 2000.
- [5] T. M. Kijek, C. A. Rossi, D. Moss, R. W. Parker, and E. A. Henschal, "Rapid and sensitive immunomagnetic-electrochemiluminescent detection of staphylococcal enterotoxin B," *J. Immunological Methods*, vol. 236, no. 1–2, pp. 9–17, 2000.
- [6] D. L. Gatto-Menking, H. Yu, B. Hao, G. John, M. T. Goode, M. Miller, and A. W. Zulich, "Preliminary testing and assay development for biotoxoids, viruses and bacterial spores using the ORIGEN immunomagnetic electrochemiluminescence sensor," in *Proc. ERDEC Scientific Conf. Chem. Biol. Defense Res.*, Aberdeen Proving Ground, MD, Nov. 1996, pp. 15–18.
- [7] R. M. Carter, R. C. Blake, T. D. Nguyen, and L. A. Bostanian, "Near real-time biosensor-based detection of 2,4-dinitrophenol," *Biosensors Bioelectron.*, vol. 18, no. 1, pp. 69–72, 2003.
- [8] A. Ahmad, A. Ramakrishnan, M. A. McLean, and A. P. Breaux, "Use of surface plasmon resonance biosensor technology as a possible alternative to detect differences in binding of enantiomeric drug compounds to immobilized albumins," *Biosensors Bioelectron.*, vol. 18, no. 4, pp. 399–404, 2003.
- [9] L. Rasooly and A. Rasooly, "Real time biosensor analysis of staphylococcal enterotoxin A in food," *Int. J. Food Microbiol.*, vol. 49, no. 3, pp. 119–127, 1999.
- [10] E. Howe and G. Harding, "A comparison of protocols for the optimization of detection of bacteria using a surface acoustic wave (SAW) biosensor," *Biosensors Bioelectron.*, vol. 15, no. 11–12, pp. 641–649, 2000.
- [11] R. Shah and N. L. Abbott, "Principles for measurement of chemical exposure based on recognition-driven anchoring transitions in liquid crystals," *Science*, vol. 293, no. 5533, pp. 1296–1299, 2001.
- [12] J. Brake, M. Daschner, and N. L. Abbott, "Biomolecular interactions at phospholipid decorated surfaces of thermotropic liquid crystals," *Science*, vol. 302, no. 5653, pp. 2094–2097, 2003.
- [13] R. R. Shah and N. L. Abbott, "Coupling of the orientations of liquid crystals and electrical double layers formed by the dissociation of surface-immobilized salts," *J. Phys. Chem. B*, vol. 105, no. 21, pp. 4936–4950, 2001.
- [14] R. R. Shah and N. L. Abbott, "Using liquid crystals to image reactants and products of acid-base reactions on surfaces with micrometer resolution," *J. Amer. Chem. Soc.*, vol. 121, no. 49, pp. 11300–11310, 1999.
- [15] Z. Hou, N. L. Abbott, and P. Stroeve, "Self-assembled monolayers on electroless gold impart pH-responsive transport of ions in porous membranes," *Langmuir*, vol. 16, no. 5, pp. 2401–2404, 2000.
- [16] V. K. Gupta and N. L. Abbott, "Uniform anchoring of nematic liquid crystals on self-assembled monolayers formed from alkanethiols on obliquely deposited films of gold," *Amer. Phys. Soc. Phys. Rev. E*, vol. 54, no. 5, pp. 4540–4543, 1996.
- [17] V. K. Gupta, T. B. Dubrovsky, and N. L. Abbott, "Optical amplification of ligand-receptor binding using liquid crystals," *Science*, vol. 279, no. 5359, pp. 2077–2080, 1998.
- [18] J. A. Van Nelson, S. R. Kim, and N. L. Abbott, "Amplification of specific binding events between biological species using lyotropic liquid crystals," *Langmuir*, vol. 18, no. 13, pp. 5031–5035, 2002.
- [19] J. J. Skaife and N. L. Abbott, "Quantitative interpretation of the optical textures of liquid crystals caused by binding of immunoglobulins to surface-bound antigens," *Langmuir*, vol. 16, no. 7, pp. 3529–3536, 2000.
- [20] R. G. Lindquist, A. Abu-Abed, and C. Woo-Hyuck, "Liquid crystal sensors with capacitive transduction," in *Proc. 5th IEEE Conf. Sensors*, Daegu, Korea, 2006, pp. 1341–1344.
- [21] J. S. Kim and D. G. Lee, "Analysis of dielectric sensors for the cure monitoring of resin matrix composite materials," *Sens. Actuators B*, vol. 30, pp. 159–164, 1996.
- [22] A. Yariv and P. Yeh, *Optical Waves in Crystals, Propagation and Control of Laser Radiation*. New York: Wiley, 2003.
- [23] M. N. Sadiku, *Numerical Techniques in Electromagnetics*, 2nd ed. Boca Raton, FL: CRC, 2001.
- [24] P. J. Collings, *Liquid Crystals, Nature's Delicate Phase of Matter*, 2nd ed. Princeton, NJ: Princeton Univ. Press, 2002.



Alaeddin Abu-Abed (S'04) received the B.Sc. and M.Sc. degrees in electrical engineering from the Jordan University of Science and Technology, Irbid, in 1999 and 2001, respectively. He is currently working towards the Ph.D. degree at the Department of Electrical and Computer Engineering, University of Alabama (UAH), Huntsville.

Since 2004, he has been a Graduate Research Assistant in the Nano and Micro Device Center (NMDC), UAH. His research interests include microdevices and nanodevices, liquid crystal devices and sensors, nanophotonics, and wireless communication.



Robert G. Lindquist received the Ph.D. degree from The Pennsylvania State University, Philadelphia, in 1992.

He is presently the Director of the Center for Applied Optics and a Professor of Electrical and Computer Engineering at The University of Alabama, Huntsville. His major research interests include liquid crystal devices for optical networking, chemical and biological sensors using liquid crystals, electronics on glass, photonics, and micro and nanofabrication technologies. Prior to UAH,

he worked for Corning Incorporated, where he managed a liquid crystal development group and worked as a Senior Research Scientist.

Woo-Hyuck Choi received the M.S. degree in electrical engineering from the University of Alabama, Huntsville, in 2006.